RSC Advances

PAPER

View Article Online
View Journal | View Issue

Cite this: *RSC Adv.*, 2020, **10**, 16330

Facile fabrication of highly flexible and floatable Cu_2O/rGO on Vietnamese traditional paper toward high-performance solar-light-driven photocatalytic degradation of ciprofloxacin antibiotic

Le Thi Thanh Nhi,[ab] Le Van Thuan,[ab] Dao My Uyen,[ab] Minh Hiep Nguyen,[c] Vu Thi Thu,[d] Dinh Quang Khieu*[e] and Le Hoang Sinh*[ab]

Received 27th February 2020
Accepted 8th April 2020

DOI: 10.1039/d0ra01854f

rsc.li/rsc-advances

In this work, we successfully demonstrated the facile fabrication of highly flexible and floatable Cu_2O/rGO on Vietnamese traditional paper (VTP) for the solar-light-driven photocatalytic degradation of the antibiotic ciprofloxacin. The catalyst membrane was prepared by the green reduction of both $Cu(OH)_2$ to Cu_2O nanoparticles and graphene oxide to reduced graphene oxide. VTP has a fibrous structure with tiny fibers connected like a spider web and multiple layers in the form of a multidimensional array, which functions as a flexible and highly porous supporter to the catalyst. Moreover, the microfibrillated cellulose of VTP acts as micro-capillaries to drag ciprofloxacin (CIP) close to the active sites on the Cu_2O/rGO/VTP surface, which improves the adsorption capacity and photocatalytic efficiency of ciprofloxacin. The adsorption process is best described by the pseudo-first-order and Freundlich models. The maximum photodegradation of CIP by the catalyst is more than 80% attained after 1.5 h under solar light irradiation with a fixed CIP concentration of 10 mg L^{-1}. The catalyst membrane exhibited good reusability of up to 5 cycles.

1. Introduction

Antibiotic residues have been considered as a serious pollutant in the aquatic environment at even very low concentrations.[1] With high toxicity, they are harmful to the human body after entering the food chain.[2] Moreover, they are difficult to photo- or bio-degrade without special treatments. Among the antibiotics, ciprofloxacin (CIP) is one of the most useful compounds of the fluoroquinolone antibiotics, which is widely used for treating some bacterial infections. The CIP residue in water and wastewater has been reported with a concentration in a range from μg L^{-1} to mg L^{-1}.[3] After drinking CIP-contaminated water, the human body loses the ability to fight against infections.[4] This is why it is critically important to remove CIP to safe concentrations in the wastewater. Several methods for the removal of CIP from aqueous solutions have been reported to date, such as coagulation, adsorption, nano-filtration membranes, and biological degradation.[5] However, the photocatalytic degradation of CIP is considered the most effective and eco-friendly method, which utilizes sunlight to convert CIP to its less or non-harmful products without the use of any toxic chemical reagents.[6] Generally, nano-sized metal oxides are used as the catalysts for a photocatalytic degradation process.[7] Nano-sized titanium dioxide (TiO_2) has been widely used as a photocatalyst for the photocatalytic degradation process.[8] However, its large bandgap energy (*ca.* 3.2 eV) limits its adsorption of solar radiation to the UV light range, which accounts for only 5% of the solar spectrum.[9] Low-cost cuprous oxide (Cu_2O) with a bandgap energy of 2.2 eV has been developed as a promising catalyst for the photocatalytic degradation process, which works in the visible light radiation that constitutes a large fraction of the solar spectrum.[10,11] However, the rapid recombination of the photogenerated electron–hole pairs limits the practical application of the Cu_2O nanostructure in photocatalytic degradation.[12] The combination of Cu_2O with other compounds *via* doping,[5] modified compositions,[10] and the formation of heterogeneous junctions[13] has been reported to prevent the recombination of photoelectrons and holes, leading to the improvement in catalysis and enhanced practical applications in visible light and sunlight. The Cu_2O composites and reduced

[a]*Center for Advanced Chemistry, Institute of Research and Development, Duy Tan University, 03 Quang Trung, Da Nang, Vietnam. E-mail: lehoangsinh@duytan.edu.vn*
[b]*Faculty of Natural Sciences, Duy Tan University, 03 Quang Trung, Da Nang, Vietnam*
[c]*Center of Radiation Technology and Biotechnology, Nuclear Research Institute, 01 Nguyen Tu Luc, Dalat, Vietnam*
[d]*University of Science and Technology of Hanoi (USTH), Vietnam Academy of Science and Technology (VAST), 18 Hoang Quoc Viet, Cau Giay, Hanoi, Vietnam*
[e]*University of Sciences, Hue University, 77 Nguyen Hue, Hue, Vietnam. E-mail: dqkhieu@hueuni.edu.vn*

graphene oxide (rGO) have been developed by many research groups as effective photocatalysts for the degradation of organic pollutants.[14–18] Previous studies have found the synergistic effects of Cu_2O and rGO in their composite form.[16,18] In particular, the superior electrical conductive rGO sheets can function as an electron collector and transporter to lengthen the charge-carrier lifetime, leading to improvements in the photocatalytic performance. The rGO sheets also extract organic pollutants from the solution to increase the contact area between the catalysts. Moreover, the Cu_2O nanoparticles prevent the restacking of rGO sheets during operation to give high performance and reusable catalysts.

Herein, a facile method was developed to synthesize flexible, highly porous, and floatable Cu_2O/rGO photocatalysts on Vietnamese traditional paper (VTP) by the co-reduction of $Cu(OH)_2$ and graphene oxide (GO) in an alkali solution toward the high performance solar-light-driven photocatalytic degradation of the antibiotic ciprofloxacin. VTP is one of the most famous papers in Vietnam, which was produced from the bark of Do trees through the traditional manual process in Vietnam. This paper has a fibrous structure and tiny fibers connected like a spider web and is multi-layered in the form of a multidimensional array. In this study, the main ingredient of VTP was cellulose with an abundance of oxygen functional groups on the surface. The VTP functioned as a flexible and highly porous supporter of the catalyst. Moreover, the presence of the microfibrillated cellulose of VTP served as micro-capillaries to drag CIP close to the active sites of Cu_2O/rGO/VTP, which improved the adsorption capacity and photocatalytic efficiency of CIP. The experiments of the adsorption and the photo-degradation for CIP were observed in detail. Finally, the regeneration of Cu_2O/rGO/VTP was also evaluated for long-term applications.

2. Experimental section

2.1 Materials

Graphite (flake sizes > 500 μm) and ciprofloxacin ($C_{17}H_{18}FN_3O_3$, >98%) were purchased from Sigma Aldrich. Copper(II) sulfate pentahydrate ($CuSO_4 \cdot 5H_2O$, 98.0%), sodium hydroxide (NaOH, 97%), ascorbic acid ($C_6H_8O_6$, 99.0%), sulfuric acid (H_2SO_4, 98%), sodium nitrate ($NaNO_3$, 99%), potassium permanganate ($KMnO_4$, 99%), hydroperoxide (H_2O_2, 30%), and hydrochloric acid (HCl, 35%) were obtained from Merck (Germany). All chemicals were used as analytical reagents without further purification.

2.2 Preparation of Cu_2O/rGO/VTP

The synthesis of the GO solution from natural graphite by the modified Hummer's method was described in our previous work.[19] The preparation of the Cu_2O/rGO/VTP membrane involved a three-step process. First, the GO/VTP membrane was fabricated by coating the GO solutions (4 mg mL^{-1}) on the VTP of the dual faces and drying at 60 °C for 30 min. The obtained membrane was cut into small pieces of equal size (2 cm × 2 cm). Second, the small GO/VTP membranes were immersed into the $CuSO_4 \cdot 5H_2O$ solution (0.05 M) for 2 h, and reduced by a 30 mL mixture of NaOH at 0.2 M and ascorbic acid at 0.1 M (with a volume ratio of 2 : 1) at 60 °C for 2 h. Finally, the resulting membranes were washed by distilled water to remove any residual base and acid, and followed with drying at room temperature.

2.3 Characterizations

The morphologies of the as-prepared materials were characterized by field emission scanning electron microscope (FESEM; S-4800, Hitachi) operated at 5.0 kV accelerating voltage. The crystal structures and phase purities were analyzed by X-ray powder diffraction (XRD; D5005, Siemens) with Cu-Kα radiation ($k = 1.1506$ Å), a 2-theta scanning range of 5–75° at 40 kV, and a current of 30 mA. Fourier transform infrared spectroscopy (FTIR; Nicolet 6700, Thermo Scientific) was used to identify the functional groups on the materials. Elemental analysis was carried out by an energy-dispersive X-ray (EDX) spectroscopy (connected with FESEM; S-4800, Hitachi). Raman spectra were observed with an Xplora Plus Raman system (Horiba, Japan) equipped with a cooled CCD detector (−60 °C) and edge filter.

2.4 Adsorption experiments

The adsorption experiments were observed by immersing a Cu_2O/rGO/VTP membrane (2 × 2 cm^2) in 10 mL CIP solutions of different initial concentrations. The pH of the solutions was maintained at the required pH by adding 0.1 M of NaOH or 0.1 M HCl. The membrane with the CIP solution was shaken for 4 h, and the CIP concentrations in the solutions at selected contact times were determined by a UV-Vis Spectrophotometer at 265 nm. The capacity adsorption of CIP at the equilibrium (q_e, mg g^{-1}) and the removal efficiency (R, %) were calculated by the following equations:

$$q_e = \frac{(C_0 - C_e)V}{w} \quad (1)$$

$$R = \frac{(C_0 - C_e)}{C_0} \times 100 \quad (2)$$

where C_0 and C_e are the initial and final concentrations of the CIP solutions (mg L^{-1}), V is the volume of the CIP solutions (L), and w is the weight of the Cu_2O/rGO/VTP membrane (g). All results of the adsorption experiments were the average values of triplicate measurements.

2.5 Photocatalytic degradation of CIP

The photocatalytic degradation of CIP was analyzed by adding Cu_2O/rGO/VTP with size (2 × 2 cm^2) into a Petri dish (diameter = 70 mm) that contained 10 mL CIP solution of different concentrations (5–20 mg L^{-1}). The adsorption experiments were done in the dark for 4 h to obtain the equilibrium adsorption of CIP onto the photocatalyst. At the end of the adsorption, the concentration of the CIP solutions was determined by a UV-Vis spectrophotometer at 265 nm and taken as the initial concentration (C_0, mg L^{-1}) for the photocatalytic degradation experiment. The degradation of CIP was then carried out under

sunlight for 2.5 h. All photo-catalytic degradation experiments were carried out in triplicate.

3. Results and discussion

3.1 Fabrication of Cu_2O/rGO/VTP

The fabrication process of Cu_2O/rGO/VTP is schematically illustrated in Fig. 1a. The VTP sheet with a size of 10 cm × 20 cm was placed onto a substrate. The viscous GO solution was coated on VTP, followed by drying at 60 °C overnight. The dried GO/VTP sheet was immersed in a $CuSO_4$ solution for 2 h to maximize the adsorption of the Cu^{2+} ions onto the GO surfaces. The sheet was then reduced *in situ* by adding a mixture of NaOH and ascorbic acid to reduce GO to rGO and convert Cu^{2+} to Cu_2O nanoparticles on the formed rGO surface. The amounts of rGO and Cu_2O on the dried Cu_2O/rGO/VTP membrane were determined to be 1.25 mg cm^{-2} and 1.75 mg cm^{-2}, respectively.

The mechanism of Cu_2O nanoparticle formation on rGO/VTP can be followed according to two main reactions:

$$CuSO_4 + 2NaOH \rightarrow Cu(OH)_2 + Na_2SO_4 \quad (3)$$

$$Cu(OH)_2 + C_6H_8O_6 \rightarrow Cu_2O + C_6H_6O_6 + H_2O \quad (4)$$

The Cu^{2+} ions were first precipitated on the GO sheets as $Cu(OH)_2$ nanoparticles. The formed $Cu(OH)_2$ nanoparticles were then reduced to Cu_2O nanoparticles with the simultaneous reduction of GO to rGO.

The FESEM images of VTP, rGO/VTP, and Cu_2O/rGO/VTP are shown in Fig. 1c–e. VTP contains closely connected cellulose fibrils with the diameter in a range of 10 to 25 μm, which provides its ductile property. After coating GO layer-by-layer on VTP and reduction by ascorbic acid, the FESEM image of rGO/VTP showed the thin regular layer of rGO on VTP (Fig. 1d). In addition, the co-reduction of GO and $CuSO_4$ took place to form Cu_2O/rGO/VTP with a dense distribution of Cu_2O nanoparticles of diameter from 25 nm to 50 nm on the surface of rGO/VTP as in Fig. 1e indicating a lot of available adsorption sites on the surface. The inset in Fig. 1e shows the EDX spectrum of Cu_2O/rGO/VTP, indicating the presence of the C, O, and Cu elements with compositions of 20.89, 32.75 and 46.36%, respectively. This implied that Cu_2O was successfully decorated on the Cu_2O/rGO/VTP membrane.

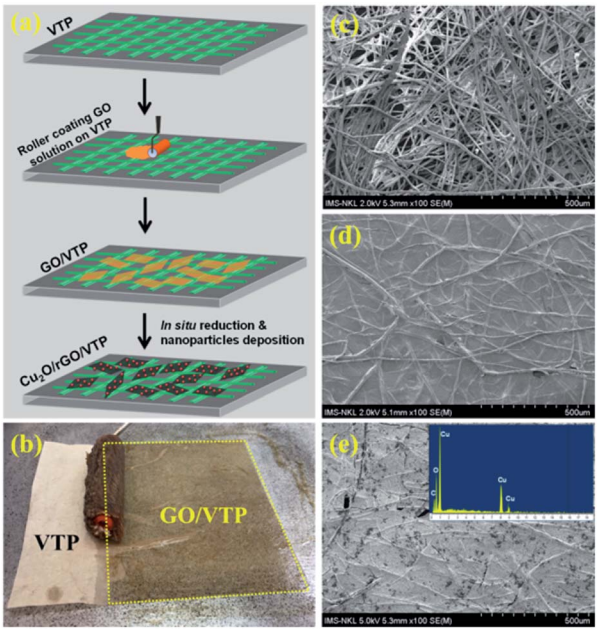

Fig. 1 Fabrication of the Cu_2O/rGO/VTP photocatalyst: (a) schematic illustration of the fabrication of the photocatalyst by the roller coating method; (b) photograph of a VTP sheet coated with GO solution; (c–e) SEM images of VTP (c), GO/VTP (d), and Cu_2O/rGO/VTP (e).

3.2 Characterizations of Cu_2O/rGO/VTP

To more deeply investigate the morphology of the photocatalyst membrane, the SEM images of rGO/VTP and Cu_2O/rGO/VTP are shown in Fig. 2a–d. The SEM image of rGO/VTP shows that the GO sheets adhere strongly to the cellulose filaments of VTP (Fig. 1a). Moreover, the wrinkles on the GO sheets at the attachment site to the cellulose filaments are observed at higher magnification (Fig. 2b). This can be explained by differences in the shrinking of the GO sheets and cellulose filaments during the drying process. The Cu_2O nanoparticles uniformly covered most areas of rGO/VTP, indicating the good adhesion between them (Fig. 2c and d). The crystalline phases of GO, VTP, GO/VTP, rGO/VTP and Cu_2O/rGO/VTP were analyzed by X-ray diffraction, and the results are shown in Fig. 2e. The XRD pattern of VTP shows the presence of microcrystalline cellulose with characteristic peaks at 2θ of 14.8° and 22.7°, corresponding to the (110) and (200) planes. The reduction from GO/VTP to rGO/VTP was completed due to the existence of the peak at 2θ of 25.5°.[20] In the XRD pattern of Cu_2O/rGO/VTP, it can be seen that Cu_2O was clearly characterized *via* the main peaks at $2\theta = 29.5°$, 36.4°, 42.3°, and 61.3° corresponding to the (110), (111), (200) and (220) crystallographic planes, respectively, of cubic Cu_2O (JCPDF 05-0667).[21] The FTIR spectra of VTP, rGO/VTP, and Cu_2O/rGO/VTP provided the structural information and are depicted in Fig. 2f. The VTP sample was produced from the Do tree (*Rhamnoneuron balansae*) of Vietnam in which cellulose is the main constituent. The respective characteristic peaks of cellulose in VTP were observed in the FTIR spectra of the three samples, such as O–H (3339 cm^{-1} and 1654 cm^{-1}), C–H (2901 cm^{-1}) and C=O (1030 cm^{-1}).[22] Compared to the VTP and rGO samples, the symmetrical stretching band of the O–H group of rGO/VTP increased both the intensity and width of the peak at 3339 cm^{-1}. Moreover, the peak for O–H bending shifts from 1654 cm^{-1} of VTP to 1572 cm^{-1} of rGO/VTP. This can be attributed to a strong hydrogen bond interaction between VTP and rGO.[22,23] The Raman spectra were used to characterize rGO in rGO/VTP and Cu_2O/rGO/VTP, and the results were shown in Fig. 2g. The two characteristic peaks of rGO appeared clearly in rGO/VTP and Cu_2O/rGO/VTP, such as the D band (1346 cm^{-1}) and G band (1596 cm^{-1}) with different ratios.[18] The D and G bands correspond to the breathing modes of rings or *k*-point photons of A_{1g} symmetry and E_{2g}, respectively, and in-plane bond stretching of pairs of sp^2-bonded carbon atoms.[24] The

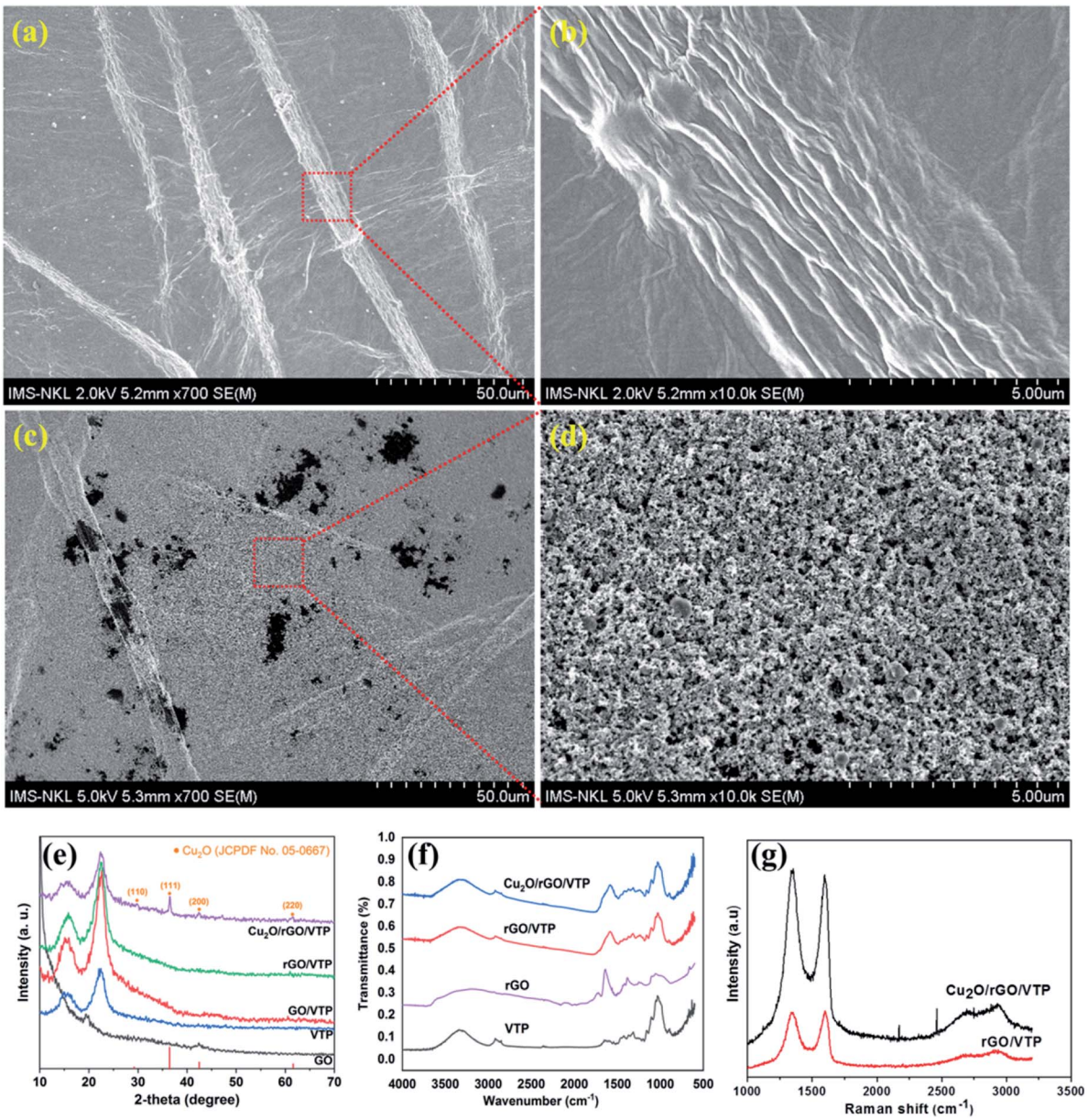

Fig. 2 Characterizations of the Cu_2O/rGO/VTP photocatalyst: (a and b) SEM images of GO/VTP at a magnification of 700× (a) and 10k× (b); (c and d) SEM images of Cu_2O/rGO/VTP at 700× (c) and 10k× (d); (e) XRD spectra of the samples; (f) FTIR spectra of the samples; (g) Raman spectra of the samples.

ratio of I_D/I_G for GO/VTP is 0.99, which is slightly smaller than that for Cu_2O/rGO/VTP at 1.04. This indicates the propagation of the sp^2 domains on the GO surface during reduction with ascorbic acid.

3.3 Adsorption of CIP

Fig. 3a shows the high elasticity and flexibility of the floatable catalyst membranes, which are recovered rapidly after folding. The pH of the reaction solution significantly affected the adsorption capacity of the Cu_2O/rGO/VTP membranes, which involved charging accumulations on the Cu_2O/rGO/VTP surface and ion species of ciprofloxacin ions. The pH value is the point where the negative and positive surface concentrations are equal, *i.e.*, the surface is electrically neutral, is called the point of zero charges (pH_{PZC}).[25] As shown in Fig. 3b, the pH_{PZC} of the Cu_2O/rGO/VTP membrane is 6.5. CIP is an ampholytic compound with a pK_a value of 6.1 for the carboxylic group and 8.7 for the nitrogen on the piperazinyl ring.[26] As a result, CIP exists in three forms depending on the pH of the reaction solution: a cationic form at pH values lower than 6.1, a zwitterionic form in the pH range of 6 to 9, and an anionic form at a pH value higher than 9 (see the inset of Fig. 3b). Thus, we investigated the adsorption of CIP on the Cu_2O/rGO/VTP surface at the three pH values of 4, 7, and 10 according to these three regions and the data are shown in Fig. 3c. The adsorption of CIP on the Cu_2O/rGO/VTP surface showed the same tendency for all pH

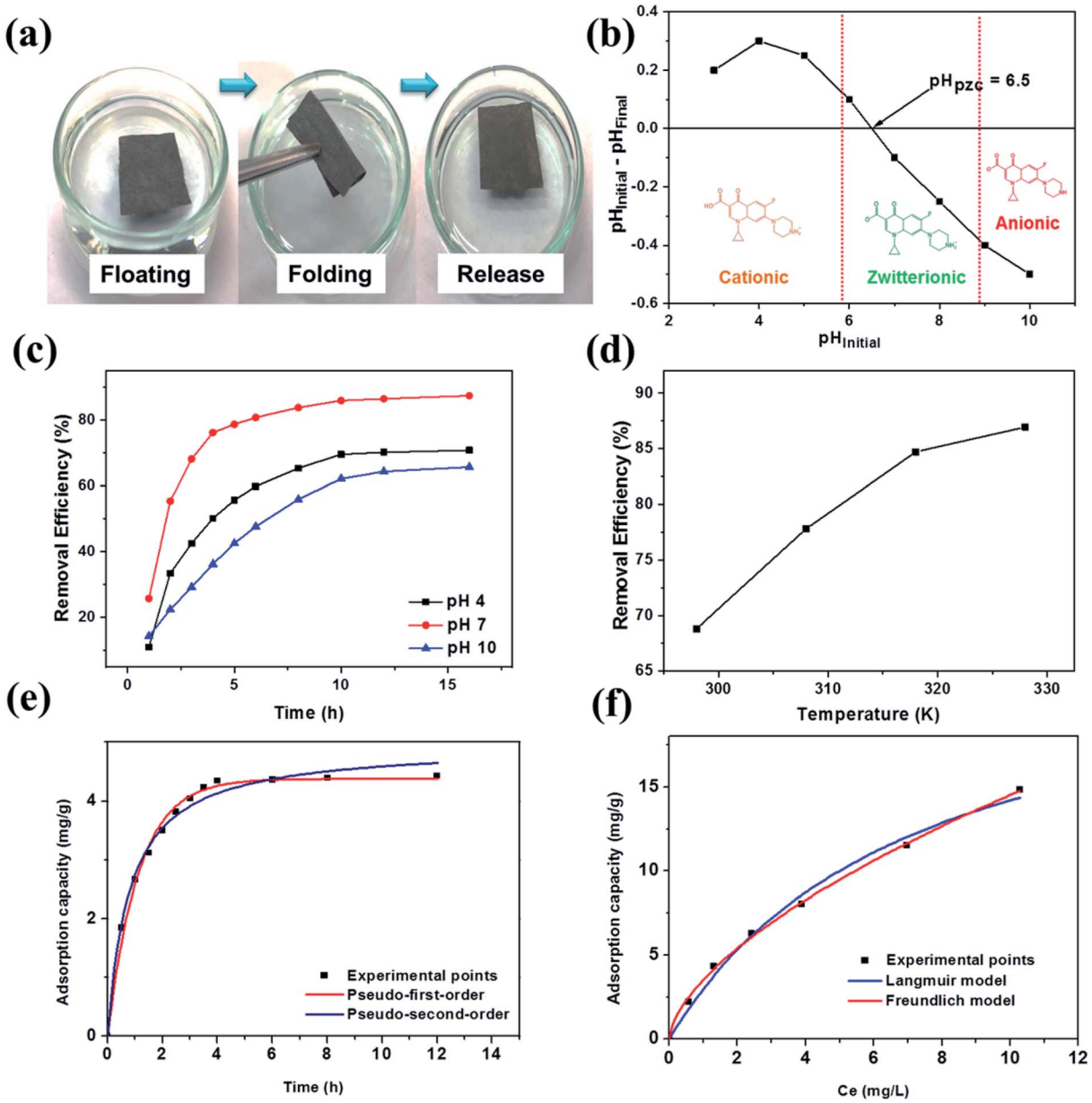

Fig. 3 Adsorption of CIP onto Cu_2O/rGO/VTP: (a) illustration of the highly flexible and floatable catalyst membrane; (b) the point of zero charge (PZC) of the catalyst; (c) the effects of pH on the removal efficiency of CIP by the catalyst; (d) the effects of temperature on the removal efficiency of CIP by the catalyst, (e) plot of fitting between the experimental data to the pseudo-first-order and the second-order adsorption models; (f) plot of fitting between the experimental data to the Langmuir and Freundlich isotherm models.

values, which got a fast adsorption rate within the first 5 h and increased slowly thereafter. The adsorptions were saturated after 15 h. The removal efficiency was highest when the pH of the reaction solution was at pH = 7. This can be attributed to the kind of charges of the catalyst surface and CIP molecule at each pH value. With a pH at 4, the protonated catalyst surface does not favor adsorption of the cationic form of CIP, resulting in low adsorption. When the pH value is at 10, the catalyst surface brings negative charges, leading to a decrease of adsorption of the anionic form of CIP at this pH value. The maximum adsorption was found at a pH of 7 owing to the strong electrostatic interaction of the zwitterionic form of CIP to the slightly negative charge of the catalyst surface. This agrees well with other reported results on the adsorption of CIP carbonaceous adsorbents.[27–29] The effect of temperature on the removal efficiency of CIP by Cu_2O/rGO/VTP is shown in Fig. 3d in a temperature range of 25 °C to 55 °C and a fixed concentration of CIP at 40 mg L^{-1}. The removal efficiency of CIP by Cu_2O/rGO/VTP increased from 68.8% at 25 °C to 87.0% at 55 °C. This can be attributed to the adsorption process, chemisorption, which is an endothermic process, and leads to an increase of the adsorption of CIP onto Cu_2O/rGO/VTP. Moreover, the increasing mobility of the CIP molecules at a higher temperature may also contribute to improving the adsorption capacity.[30]

The pseudo-first-order and second-order adsorption models, as well as two important isotherm models (Langmuir and Freundlich), were used to explain the experimental data obtained from the effect of the contact time in the concentration of CIP at 10 mg L^{-1}. This investigation finds the best fitted kinetic and isotherm model, which provides information about the adsorption mechanism and the rate of CIP adsorption onto Cu_2O/rGO/VTP. In particular, the equations of the pseudo-first-order and pseudo-second-order kinetic models, Langmuir and Freundlich isotherm models, were described as eqn (5), (6), (7) and (8), respectively.

$$q_t = q_e(1 - e^{-k_1 t}) \quad (5)$$

$$q_e = \frac{q_e^2 k_2 t}{1 + q_e k_2 t} \quad (6)$$

$$q_e = \frac{q_m K_L C_e}{1 + K_L C_e} \quad (7)$$

$$q_e = K_F C_e^{1/n} \quad (8)$$

where q_t (mg g^{-1}) and q_e (mg g^{-1}) were the amounts of CIP adsorbed onto the adsorbent at time t (min) and at equilibrium; k_1 (h^{-1}) and k_2 (g mg^{-1} h^{-1}) are the rate constants of the first and second-order adsorptions; C_e is the equilibrium concentration of CIP (mg L^{-1}), q_e is the amount of CIP adsorbed per unit weight of adsorbent (mg g^{-1}), q_m is the maximum adsorption capacity of Cu_2O/rGO/VTP for CIP (mg g^{-1}), K_L is the Langmuir equilibrium constant (L mg^{-1}); K_F (mg g^{-1}) and n are the Freundlich equilibrium constants. The range of the n value from 1 to 10 implied that the adsorption was favorable.[31]

The fitting of the experimental data with the adsorption models and isotherm models are shown in Fig. 3e and f, respectively. Moreover, the calculated data are presented in Table 1. The correlation coefficient R^2 of the pseudo-first-order model (0.992) was higher than that of the pseudo-second-order model (0.251). Furthermore, the calculated value of the adsorption capacity of the pseudo-first-order kinetic model ($q_{e(cal)}$ = 4.38 mg g^{-1}) is closer to the experimental value ($q_{e(exp)}$ = 4.43 mg g^{-1}) than that of the pseudo-second-order model (4.96 mg g^{-1}). These results indicate that the adsorption kinetic processes of CIP onto Cu_2O/rGO/VTP were better described by the pseudo-first-order model. Thus, the rate of CIP adsorption on this material was directly proportional to the difference between the adsorption capacity at any time t and the adsorption capacity at equilibrium.[25] A similar result was also reported by the previous study.[30]

In order to determine the adsorption mechanism of CIP onto Cu_2O/rGO/VTP, the adsorption isotherm is an important parameter to indicate the distribution of adsorbates between the solid phase and liquid phase when the adsorption reaches an equilibrium state.[32] According to Table 1, the results show that both Langmuir and Freundlich isotherm models fit the experimental data well with very high correlation coefficients R^2. However, the correlation coefficient for the Freundlich model (R^2 = 0.998) was higher than that for the Langmuir model (R^2 = 0.990), indicating that the adsorption process was best followed by the Freundlich model. This isotherm model presented concordantly the adsorption processes that occur as multilayers on the heterogeneous surfaces.[33] The value of parameter n in the Freundlich model is 1.63 (in the range from 1 to 10), indicating that the adsorption of CIP onto Cu_2O/rGO/VTP is a favorable process. The maximum adsorption capacity q_m of CIP onto Cu_2O/rGO/VTP calculated from the Langmuir equation is 24.50 mg g^{-1}.

Table 1 Isotherm and kinetic parameters for the adsorption of CIP on Cu_2O/rGO/VTP

Isotherm model	Value	Kinetic model	Value
Langmuir model		**Pseudo-first-order**	
q_m (mg g^{-1})	24.50	$q_{e(cal)}$ (mg g^{-1})	4.38
K_L (L mg^{-1})	0.138	k_1 (min^{-1})	0.895
R^2	0.990	R^2	0.992
Freundlich model		**Pseudo-second-order**	
K_F (mg g^{-1})	3.52	$q_{e(cal)}$ (mg g^{-1})	4.96
n	1.63	k_2 (min^{-1})	0.898
R^2	0.998	R^2	0.251

3.4 Kinetics of the photocatalytic degradation of CIP

Kinetic studies provide necessary information for investigating the adsorption process, which is used to determine the adsorption rate and the equilibrium time. Kinetic experiments of photodegradation of CIP were conducted in four different reaction solutions in the presence of VTP, rGO/VTP, Cu_2O/rGO/VTP, and the control solution containing only CIP. The C/C_0 ratios were plotted as a function of reaction times up to 2.5 h as in Fig. 4a. The CIP was slightly photodegraded under sunlight. With the presence of VTP and rGO/VTP, the concentration of CIP decreased after 2.5 h due to the adsorption of the adsorbent, indicating that the cellulose in VTP with the oxygen functional groups slowly reacted with CIP due to the electron accumulation on the VTP surface. With the presence of Cu_2O/rGO/VTP, an effective photodegradation of CIP was observed with only 17% CIP left after 2.5 h reaction. The highly effective degradation of CIP by Cu_2O/rGO/VTP is attributed to an efficient charge transfer from Cu_2O to rGO, which improved the separation efficiency of the light-stimulated carriers, as well as the photocatalytic activity and stability.[34] The rate constant of photodegradation was calculated as shown in the following equation:

$$\ln\left(\frac{C_0}{C}\right) = kt \quad (9)$$

where C_0 and C are the concentrations of CIP on the Cu_2O/rGO/VTP; and k is the rate constant (min^{-1}). The values of the rate constants for the sample without catalyst (CIP-light), VTP, rGO/VTP, and Cu_2O/rGO/VTP are shown in Fig. 4b. The degradation rate of CIP by Cu_2O/rGO/VTP was 1.16873 min^{-1}, which is much higher than that of the reaction with the presence of VTP and rGO/VTP, and the control solution without the catalyst. This

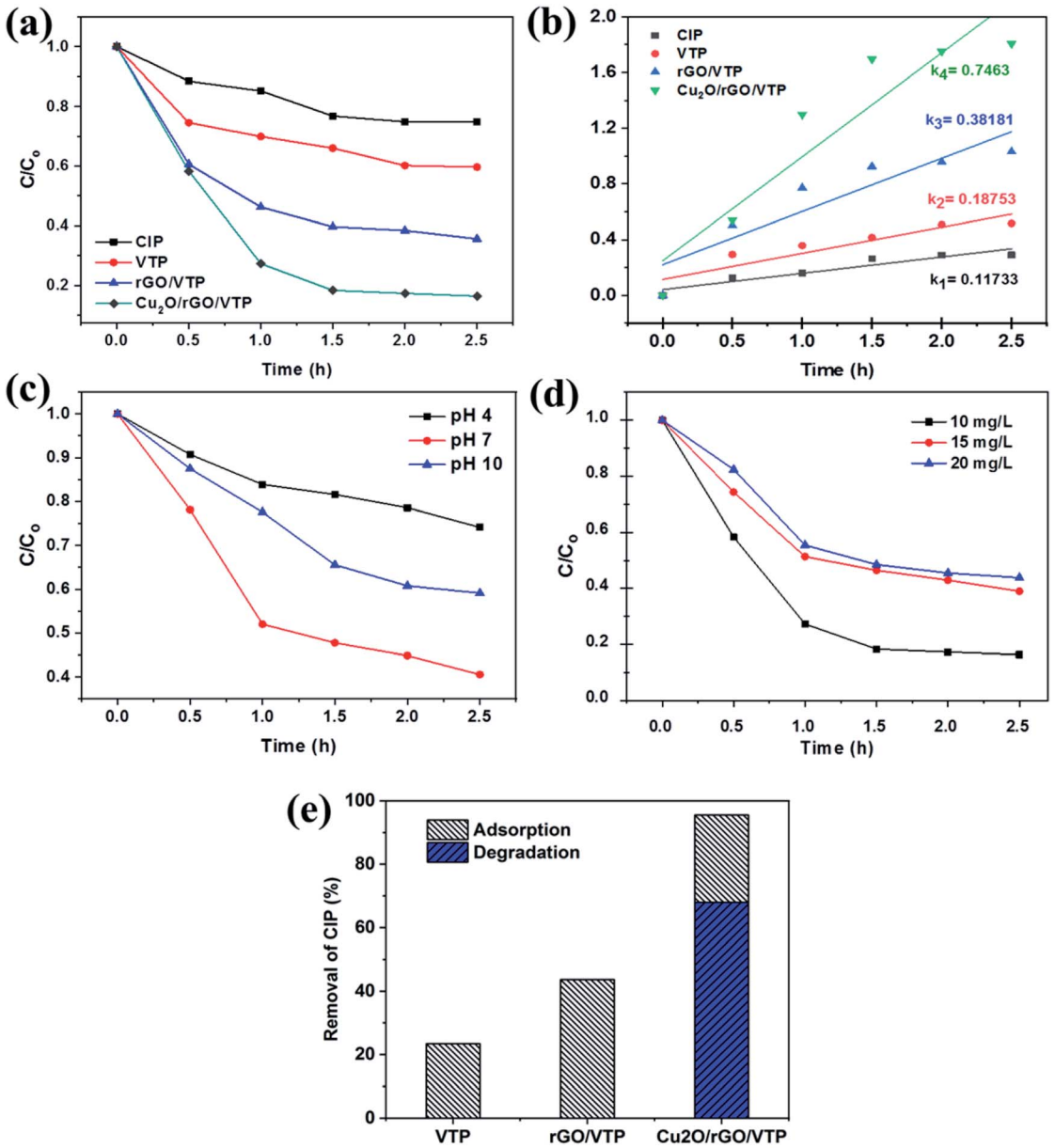

Fig. 4 The photocatalytic degradation of CIP by Cu_2O/rGO/VTP: (a) the photocatalytic degradation of CIP in the presence of VTP, rGO/VTP, Cu_2O/rGO/VTP, and without the use of a catalyst; (b) linear fitting of the photocatalytic degradation; (c) effect of pH on the photocatalytic degradation of CIP by Cu_2O/rGO/VTP; (d) effect of the CIP concentration on the photocatalytic degradation; (e) comparison of adsorption and degradation efficiencies.

implies that Cu_2O/rGO/VTP has a high degradation efficiency to CIP under sunlight.

The influence of pH on the catalytic degradation of CIP by the Cu_2O/rGO/VTP catalyst is presented in Fig. 4c. The best degradation was attained at a pH of 7, which can be explained by the highest accumulation of CIP on the surface of the catalyst at this pH value as already discussed in adsorption.

The effect of the initial CIP concentrations on the photocatalytic capacity for Cu_2O/rGO/VTP was studied at a pH value of 7 under sunlight. Fig. 4d shows the relation of the photodegradation rate and irradiation time of CIP at three different concentrations of 10, 15, and 20 mg L^{-1}. The degradation efficiencies decreased when increasing the concentration of CIP. In addition, the overall removal ability between the adsorption and photocatalysis was an important key to evaluating a balance to get the highest efficiency.[35,36] The removal of CIP in regards to the adsorption and degradation efficiency is shown in Fig. 4e, which indicates that VTP and rGO/VTP are involved in the adsorption of CIP due to the functional groups of cellulose and rGO. Cu_2O/rGO/VTP was the most capable in removing CIP in the aqueous solutions due to the presence of the semiconductor Cu_2O on the surface of the catalyst. Thus, Cu_2O/rGO/VTP is a suitable membrane that can balance

between the adsorption and degradation of CIP in solutions under sunlight with the highest efficiency.

3.5 Discussion of photocatalytic degradation

The attack of holes (h^+) and the addition of $^{\bullet}OH$ have been reported as the main pathways responsible for the photocatalytic degradation of CIP by the Cu_2O-based catalyst. Moreover, eight intermediates have been detected in the photocatalytic degradation of CIP.[37] Many previous works have also reported on the high photocatalytic performance of the Cu_2O/rGO catalyst owing to the synergistic effect of the Cu_2O nanoparticles and rGO sheets.[10,12,15,16,18,38,39] The possible mechanism of the photodegradation of CIP in this work is proposed as in Fig. 5 based on these published investigations. The important factors to determine the efficiency of the photocatalytic process are the efficient adsorption of CIP on Cu_2O/rGO/VTP and the effective separation of the photo-generated electrons/hole pairs. The Cu_2O/rGO/VTP photocatalyst can easily absorb CIP on its surface due to the presence of the –COOH and –OH groups of cellulose in VTP, as well as the oxygen functional groups of rGO. The valence electrons of Cu_2O were excited and transferred onto rGO under the sunlight irradiation, and then they acted as an electron trap.[6] The trapped electrons on rGO reacted with oxygen to create some reactive oxygen species ($^{\bullet}O_2$–, $^{\bullet}OH$), indicating that the rate of the combination of electrons and holes decreased. On the other hand, the photo-generated electrons on Cu_2O could be trapped directly with oxygen to form the reactive oxygen species. Then, water could react with them to create hydroxyl radicals, which degraded CIP with high efficiency.

3.6 Regeneration and reusability of the photocatalyst

To evaluate the reusability of the catalysts, five cycles of the photocatalytic experiments were done under sunlight using 0.02 g of adsorbents loaded into the solution with a fixed CIP concentration of 10 mg L^{-1}. After each cycle of the photocatalytic reaction, the adsorbent was separated and washed by water until the adsorption peak of CIP at 265 nm was not detected in the washing solution. The C/C_0 ratios and degradation efficiencies are shown in Fig. 6a and b. The catalyst exhibited good reusability with no significant loss of degradation efficiency after 5 cycles of uses. Moreover, the FESEM images of the as-prepared Cu_2O/rGO/VTP and after 5 photodegradation CIP cycles are shown in Fig. 6c and d. There is no visible change in the morphology of the catalyst. This indicates that it is suitable for practical applications as a photocatalyst.

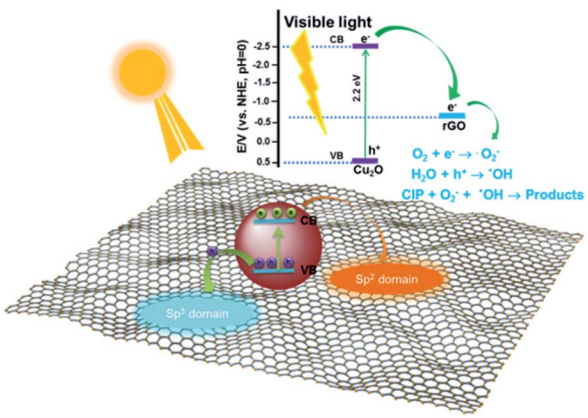

Fig. 5 Schematic illustration of the proposed reaction mechanism for CIP photodegradation by the Cu_2O/rGO/VTP catalyst under solar light irradiation.

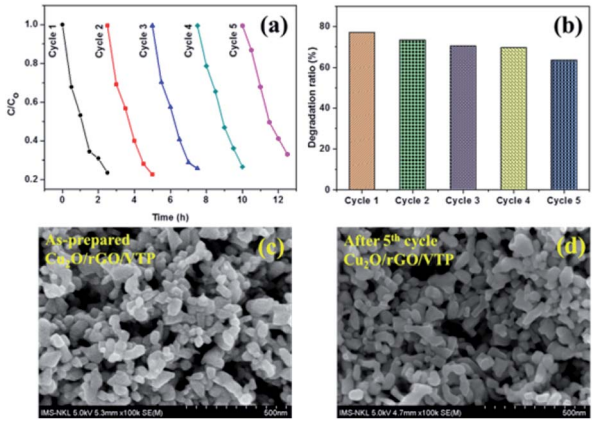

Fig. 6 Regeneration and reusability of the photocatalyst: (a) the efficiency of the photocatalytic degradation of CIP after 5 cycles; (b) degradation ratio after 5 cycles; (c and d) SEM images of the as-prepared catalyst (c) and after 5 cycles (d).

4. Conclusions

A Cu_2O/rGO/VTP membrane successfully demonstrated the solar-light-driven photocatalytic degradation of the antibiotic ciprofloxacin. The Cu_2O nanoparticles were uniformly covered on the surfaces of the rGO sheets. The catalyst membrane exhibited high flexibility and floatability, indicating its suitability for practical applications. The adsorption capacity of CIP on Cu_2O/rGO/VTP under the irradiation of sunlight was 24.50 mg g^{-1}. In addition, the photodegradation of CIP with the high rate constant was better than that of VTP and rGO/VTP. The photocatalyst demonstrated high recyclability of the adsorbent for up to five cycles. The results of this research indicated that photo-catalytic oxidation is a cost-effective method to remove antibiotics in water.

Conflicts of interest

There are no conflicts to declare.

Acknowledgements

This work was supported by the Domestic Master/PhD Scholarship Programme of the Vingroup Innovation Foundation.

References

1 Y. Ben, C. Fu, M. Hu, L. Liu, M. H. Wong and C. Zheng, *Environ. Res.*, 2019, **169**, 483–493.
2 J. Ma, M. Yang, F. Yu and J. Zheng, *Sci. Rep.*, 2015, **5**, 13578.
3 S. Shehu Imam, R. Adnan and N. H. Mohd Kaus, *Toxicol. Environ. Chem.*, 2018, **100**, 518–539.
4 M. Malakootian, A. Nasiri and M. Amiri Gharaghani, *Chem. Eng. Commun.*, 2020, **207**, 56–72.
5 M. Mirzai, F. Akhlaghian and F. Rahmani, *Water Environ. J.*, 2019, 12477.
6 M. El-Kemary, H. El-Shamy and I. El-Mehasseb, *J. Lumin.*, 2010, **130**, 2327–2331.
7 R. Gothwal and T. Shashidhar, *Clean: Soil, Air, Water*, 2015, **43**, 479–489.
8 A. Ajmal, I. Majeed, R. N. Malik, H. Idriss and M. A. Nadeem, *RSC Adv.*, 2014, **4**, 37003–37026.
9 H. Dong, G. Zeng, L. Tang, C. Fan, C. Zhang, X. He and Y. He, *Water Res.*, 2015, **79**, 128–146.
10 H. Huang, J. Zhang, L. Jiang and Z. Zang, *J. Alloys Compd.*, 2017, **718**, 112–115.
11 S. Yadav, A. Jain and P. Malhotra, *Green Chem.*, 2019, **21**, 937–955.
12 W. Zou, L. Zhang, L. Liu, X. Wang, J. Sun, S. Wu, Y. Deng, C. Tang, F. Gao and L. Dong, *Appl. Catal., B*, 2016, **181**, 495–503.
13 Y. Xia, Z. He, K. Hu, B. Tang, J. Su, Y. Liu and X. Li, *J. Alloys Compd.*, 2018, **753**, 356–363.
14 F. Han, H. Li, J. Yang, X. Cai and L. Fu, *Phys. E*, 2016, **77**, 122–126.
15 Y.-C. Pu, H.-Y. Chou, W.-S. Kuo, K.-H. Wei and Y.-J. Hsu, *Appl. Catal., B*, 2017, **204**, 21–32.
16 P. D. Tran, S. K. Batabyal, S. S. Pramana, J. Barber, L. H. Wong and S. C. J. Loo, *Nanoscale*, 2012, **4**, 3875.
17 I. Roy, A. Bhattacharyya, G. Sarkar, N. R. Saha, D. Rana, P. P. Ghosh, M. Palit, A. R. Das and D. Chattopadhyay, *RSC Adv.*, 2014, **4**, 52044–52052.
18 W. Zhang, X. Li, Z. Yang, X. Tang, Y. Ma, M. Li, N. Hu, H. Wei and Y. Zhang, *Nanotechnology*, 2016, **27**, 265703.
19 T. T. N. Le, V. T. Le, M. U. Dao, Q. V. Nguyen, T. T. Vu, M. H. Nguyen, D. L. Tran and H. S. Le, *Chem. Eng. Commun.*, 2019, **206**, 1337–1352.
20 H. Shi, W. Li, L. Zhong and C. Xu, *Ind. Eng. Chem. Res.*, 2014, **53**, 1108–1118.
21 J. Cai, W. Liu and Z. Li, *Appl. Surf. Sci.*, 2015, **358**, 146–151.
22 W. Ouyang, J. Sun, J. Memon, C. Wang, J. Geng and Y. Huang, *Carbon*, 2013, **62**, 501–509.
23 Y. J. Heo, J. W. Lee, Y. R. Son, J. H. Lee, C. S. Yeo, T. D. Lam, S. Y. Park, S. J. Park, L. H. Sinh and M. K. Shin, *Adv. Energy Mater.*, 2018, **8**, 1870120.
24 K. Wang, X. Dong, C. Zhao, X. Qian and Y. Xu, *Electrochim. Acta*, 2015, **152**, 433–442.
25 L. A. Kafshgari, M. Ghorbani and A. Azizi, *Appl. Surf. Sci.*, 2017, **419**, 70–83.
26 S. Das, S. Ghosh, A. Misra, A. Tamhankar, A. Mishra, C. Lundborg and S. Tripathy, *Int. J. Environ. Res. Public Health*, 2018, **15**, 2440.
27 T. S. Anirudhan and J. R. Deepa, *J. Colloid Interface Sci.*, 2017, **490**, 343–356.
28 Z. Movasaghi, B. Yan and C. Niu, *Ind. Crops Prod.*, 2019, **127**, 237–250.
29 E.-S. I. El-Shafey, H. Al-Lawati and A. S. Al-Sumri, *J. Environ. Sci.*, 2012, **24**, 1579–1586.
30 D. Robati, M. Rajabi, O. Moradi, F. Najafi, I. Tyagi, S. Agarwal and V. K. Gupta, *J. Mol. Liq.*, 2016, **214**, 259–263.
31 W. Konicki, M. Aleksandrzak and E. Mijowska, *Pol. J. Chem. Technol.*, 2017, **19**, 120–129.
32 M. Hasan, A. L. Ahmad and B. H. Hameed, *Chem. Eng. J.*, 2008, **136**, 164–172.
33 G. Shen, L. Pan, R. Zhang, S. Sun, F. Hou, X. Zhang and J. J. Zou, *Adv. Mater.*, 2020, **32**, 1905988.
34 X. An, K. Li and J. Tang, *ChemSusChem*, 2014, **7**, 1086–1093.
35 S. Wang, X. Zhang, L. Pan, F. M. Zhao, J. J. Zou, T. Zhang and L. Wang, *Appl. Catal., B*, 2015, **164**, 234–240.
36 G. Shen, L. Pan, Z. Lü, C. Wang, F.-E. Aleem, X. Zhang and J. J. Zou, *Chin. J. Catal.*, 2018, **39**, 920–928.
37 X. Yu, J. Zhang, J. Zhang, J. Niu, J. Zhao, Y. Wei and B. Yao, *Chem. Eng. J.*, 2019, **374**, 316–327.
38 B. Li, T. Liu, L. Hu and Y. Wang, *J. Phys. Chem. Solids*, 2013, **74**, 635–640.
39 B. M. Almeida, M. A. Melo, J. Bettini, J. E. Benedetti and A. F. Nogueira, *Appl. Surf. Sci.*, 2015, **324**, 419–431.

